LETTER

An Adaptive Multilook Approach of Multitemporal Interferometry Based on Complex Covariance Matrix for SAR Small Datasets

Jingke ZHANG[†], **Huina SONG**[††a)], **Mengyuan WANG**[††], **Zhaoyang QIU**[††], **Xuyang TENG**[††], ***Nonmembers***, ***and*** **Qi ZHANG**[†††], ***Member***

SUMMARY Adaptive multilooking is a critical processing step in multitemporal interferometric synthetic aperture radar (InSAR) measurement, especially in small temporal baseline subsets. Various amplitude-based adaptive multilook approaches have been proposed for the improvement of interferometric processing. However, the phase signal, which is fundamental in interferometric systems, is typically ignored in these methods. To fully exploit the information in complex SAR images, a nonlocal adaptive multilooking is proposed based on complex covariance matrix in this work. The complex signal is here exploited for the similiarity measurement between two pixels. Given the complexity of objects in SAR images, structure feature detection is introduced to adaptively estimate covariance matrix. The effectiveness and reliability of the proposed approach are demonstrated with experiments both on simulated and real data.

key words: *SAR, adaptive multilooking, covariance matrix*

1. Introduction

Multi-temporal interferometric synthetic aperture radar (MT-InSAR) techniques have widespread application in earth observations because of its high precision and wide coverage. MT-InSAR techniques are generally classified into two main types: permanent scatterer (PS) technique [1] and small baseline subsets (SBAS) [2]. In SBAS methods, a subset of interferograms are formed by small temporal-spatial baselines, and the deformation signal of highly correlated regions can be extracted from small SAR datasets. Multilook processing plays an important role in accurate estimation of surface elevation and surface deformation. It is helpful to reduce temporal-spatial decorrelation and improve the robustness of unwrapped phase [3], [4].

Boxcar multilook processing is efficient but reduces the spatial resolution. Besides, it also reduces the quality of the derived final geographic information in heterogeneous regions. To solve these problems, various adaptive multilook approaches have been proposed in past years [5]–[9].

The guts of adaptive multilooking is a reasonable distance measure between neighboring pixels and predictor pixel. With multitemporal SAR datasets, some statistical methods based on empirical cumulative distribution functions (CDF), such as two-sample Kolmogorov-Smirnov (KS) test and Anderson-Darling (AD) test, were introduced to early adaptive multilook approaches [6]. To improve the power of hypothesis tests, an almost self-adaptive approach was proposed without prior knowledge or scenario assumptions [7]. In [8], they explore the potential of adaptive multilook approach in the framework of SABS processing. However, the performance of these amplitude-based approaches is usually poor in the case of small SAR datasets [10].

Compared with the amplitude information, a more appropriate description of backscattered signals is the complex covariance matrix, which is an important parameter in statistical modeling of SAR images. Thus, the test statistic of covariance matrix is introduced to measure the similarity between two pixels in this work. Given the complexity of topographic features in SAR images, covariance matrix is adaptively estimated based on the selected structure feature.

This letter is organized as follows. In Sect. 2, some traditional distance measures are briefly introduced. In Sect. 3, the procedure of the presented approach is elaborated. In Sect. 4, experimental results of simulated and real data are presented. Conclusions are drawn in Sect. 5.

2. Traditional Distance Measures

The performance of adaptive multilook approach relies on the reasonable distance measure between two pixels. The class of CDF statistics, such as KS test ans AD test, have been effectively used in adaptive multilook processing.

2.1 KS Distance

The KS test is designed as a non-parametric hypothesis test and can be used to judge if two real-valued datasets differ significantly. The KS distance between two vectors $\boldsymbol{x} = (x_1, x_2, \ldots, x_M)$ and $\boldsymbol{y} = (y_1, y_2, \ldots, y_N)$ is defined as

$$d_{\mathrm{KS}}(\boldsymbol{x}, \boldsymbol{y}) = \sqrt{\frac{MN}{M+N}} \sup_t \|F_{\boldsymbol{x}}(t) - G_{\boldsymbol{y}}(t)\|, \tag{1}$$

where $F_{\boldsymbol{x}}(t)$ and $G_{\boldsymbol{y}}(t)$ denotes the cumulative distribution function (CDF) of $\boldsymbol{x}$ and $\boldsymbol{y}$, respectively. The smaller the value of the KS distance $d_{\mathrm{KS}}(\boldsymbol{x}, \boldsymbol{y})$ is, the less the statistical difference between $\boldsymbol{x}$ and $\boldsymbol{y}$.

Manuscript received October 22, 2021.
Manuscript revised March 16, 2022.
Manuscript publicized May 13, 2022.

[†]The author is with the State Key Laboratory of Complex Electromagnetic Environment Effects on Electronics and Information Systems, Luoyang, China.
[††]The authors are with Hangzhou Dianzi University, Hangzhou, China.
[†††]The author is with the No.10 Research Institute, China Electronics Technology Group Corporation, China.
a) E-mail: huinasong@hdu.edu.cn

DOI: 10.1587/transfun.2021EAL2092

2.2 AD Distance

Compared with the KS test, the AD test is a more sensitive test. The AD distance between $\boldsymbol{x}$ and $\boldsymbol{y}$ can be described as

$$d_{\mathrm{AD}}(\boldsymbol{x},\boldsymbol{y}) = \frac{MN}{M+N}\sum \frac{[F_{\boldsymbol{x}}(t)-G_{\boldsymbol{y}}(t)]^2}{H_{\boldsymbol{z}}(t)[1-H_{\boldsymbol{z}}(t)]}, \tag{2}$$

where $H_{\boldsymbol{z}}(t)$ denotes the CDF of the vector $\boldsymbol{z} = [\boldsymbol{x},\boldsymbol{y}]$. In formal (2), all values in the vectors are taken into consideration and an appropriate weight is introduced to the tails of data distribution.

2.3 PB Distance

The PB distance was first used to measure the patch similarity in nonlocal denoising methods [11], [12]. Under reasonable assumption, the PB distance between $\boldsymbol{x}$ and $\boldsymbol{y}$ can be expressed as [8]

$$d_{\mathrm{PB}}(\boldsymbol{x},\boldsymbol{y}) = \sum \log\left[\frac{x_i}{y_i}+\frac{y_i}{x_i}\right], \tag{3}$$

Likewise, the smaller the value of the PB distance $d_{\mathrm{PB}}(\boldsymbol{x},\boldsymbol{y})$ is, the less the statistical difference between $\boldsymbol{x}$ and $\boldsymbol{y}$. Note that, unlike for KS distance and AD distance, the sample size of $\boldsymbol{x}$ and $\boldsymbol{y}$ should be equal in formula (3).

3. The Proposed Approach

The proposed adaptive multilook approach is mainly divided into two steps: estimation of covariance matrix, similarity test of covariance matrix.

3.1 Estimation of Covariance Matrix

Given a stack of N coregistered SAR images, the complex vector of a generic pixel p can be described as $\boldsymbol{d}(p) = [d_1(p), d_2(p), \ldots, d_N(p)]$, where $d_i(p)$ represents the backscatter value of p in ith SAR image. Under the assumption that each simple-look complex (SLC) observation $\boldsymbol{d}(p)$ approximately follows Goodman's model, the multivariate probability density function (PDF) of $\boldsymbol{d}(p)$ can be described as [13]

$$f(\boldsymbol{d}(p)) = \frac{1}{\pi^N \det(\mathbf{C})}\exp\{-\boldsymbol{d}(p)\mathbf{C}\boldsymbol{d}^{\mathrm{H}}(p)\}, \tag{4}$$

where $(\cdot)^{\mathrm{H}}$ denotes the conjugate transpose, $\mathbf{C}$ is an $N \times N$ complex matrix and $\det(\cdot)$ denotes the determinant of a matrix. The maximum likelihood estimator of $\mathbf{C}$ is generally calculated by

$$\mathbf{C} = \frac{1}{N_q}\sum_{q\in\Omega} \boldsymbol{d}^H(q)\boldsymbol{d}(q), \tag{5}$$

where Ω denotes the set of neighborhood pixels, and N_q denotes the number of samples in set Ω. However, the backscattering observations in a preset estimation window may follow different distribution in heterogeneous SAR scenes [14]. Thus, the different structure features are firstly detected to adaptively estimate covariance matrix in this letter.

3.1.1 Isolated Scatterer Detection

In SAR images, point-wise scatterers are generated by a deterministic bounce scattering [15]. Due to the imaging mechanism of SAR, the energy of point-wise scatterers mainly spreads on the main lobe and the first sidelobe. Let $\bar{I}_c$ and $\bar{I}_r$ be the average intensity of the inner neighbourhood (including predictor pixel and four-connected pixels) and the outer neighbourhood in a preset window, respectively. The isolated scatterer ratio detector can be calculated as $\gamma_I = \frac{\bar{I}_c}{\bar{I}_r}$ [16].

For an ideal point-wise scatterer, $\bar{I}_c$ is significantly higher than $\bar{I}_r$. Thus, the predictor pixels can be considered as an isolated scatterer when γ_I is greater than a preset threshold $\gamma_{I_{\mathrm{thres}}}$.

3.1.2 Line Detection

An ideal linear structure includes three textured regions: the oriented line and two subregions. Let $\bar{I}_{1i}$ and $\bar{I}_{2i}$ be the average intensity of two subregions on both sides of ith line, respectively. For the preset multiple directions, the ratio detector in ith direction can be calculated by [18]

$$\gamma_{L_i} = \min[\frac{\bar{I}_{1i}}{\bar{I}_{2i}}, \frac{\bar{I}_{2i}}{\bar{I}_{1i}}]. \tag{6}$$

Then, the line ratio detector γ_L can be obtained by minimizing γ_{L_i} over all directions, i.e. $\gamma_L = \min_i \gamma_{L_i}$. Based on the structural features, the predictor pixels can be considered as be located on an oriented line if $\gamma_L < \gamma_{L_{\mathrm{thres}}}$. Here, $\gamma_{L_{\mathrm{thres}}}$ denotes the preset threshold, which can be estimated by the PDF of the ratio detector γ_L presented in [17] or set empirically.

3.1.3 Homogeneous Area Detection

Homogeneous area detection is a key issue for spatial adaptive speckle filtering. As stated in [17], the homogeneity of SAR scenes can be measured by the local coefficient of variation (CV), which is calculated by $\mathrm{CV} = \frac{\delta}{\mu}$, where δ and μ represent the local standard variation and mean of intensity map, repectively. The preset window can be considered as be local homogeneous if CV $<$ Cu. The value of Cu is associated with the size of the preset window.

3.1.4 Edge Detection

In Lee filter [20], 16 directional masks were used to adaptively reduce phase noise, and experimental results showed that the use of directional windows was more effective in noise suppression. Inspired by this idea, the local CV will be calculated based on the preset 16 directional masks in 9×9 window. Then the directional window with minimum

CV is selected as the most homogeneous neighborhood. In addition, the selection of directional windows was based on the temporally averaged intensity map, in order to decrease the effect of speckle noise.

3.2 Similarity Test of Covariance Matrix

The speckle noise can be suppressed by averaging neighborhood pixels at the cost of spatial resolution. In this despeckle case, the covariance matrix, which is estimated by the selected homogeneous neighborhood, is a more appropriate description of the complex backscatter signal in SAR images.

When complex vector $\boldsymbol{d}(p)$ follows a complex multivariate normal with mean 0, the covariance matrix $\mathbf{C}$ can be considered as Wishart distributed. Let $\mathbf{X} \in W_{\mathbf{C}}(N, n_x, \Sigma_x)$ and $\mathbf{Y} \in W_{\mathbf{C}}(N, n_y, \Sigma_y)$ be two Wishart matrixes. The null and alternative hypotheses of the test statistic of covariance matrix can be stated as $\mathrm{H}_0 : \Sigma_{\mathbf{X}} = \Sigma_{\mathbf{Y}}$, $\mathrm{H}_1 : \Sigma_{\mathbf{X}} \neq \Sigma_{\mathbf{Y}}$. The likelihood-ratio test statistics of $\mathbf{X}$ and $\mathbf{Y}$ can be described as

$$Q = \frac{(n_x + n_y)^{N(n_x+n_y)}}{n_x^{Nn_x} n_y^{Nn_y}} \frac{\det(\mathbf{X})^{n_x} \det(\mathbf{Y})^{n_y}}{\det(\mathbf{X}+\mathbf{Y})^{n_x+n_y}}. \tag{7}$$

The null hypothesis H_0 can be accepted when Q is larger than a proper threshold. The theoretical threshold with a constant false-alarm probability needs to be regularly updated based on the data sets. In a simple fashion, the threshold can be set empirically.

3.3 Procedure of the Proposed Approach

As analysis presented in [10], the amplitude-based multilook approaches are usually poor in the case of small stacks of SAR images. Thus, covariance matrix, which comprises of the amplitude and phase signal of complex-valued SAR images, is introduced to measure the distance between two pixels.

Since Adaptive Multilooking is carried out based on Covariance Matrix in this work, the proposed approach is abbreviated to AMCV in the following section. The flowchart of the proposed AMCV is presented in Fig. 1. The average intensity of N coregisteried images is firstly processed in temporal dimension to suppress speckle noise to some extent. The different structure features are detected based on isolated scatterer ratio detector γ_I, line ratio detector γ_L and CV. Then, the covariance matrix of each pixel is adaptively calculated based on the selected structure feature. In a preset search window, the similiarity test indicator (7) is applied to collect the set of statistically homogeneous pixels, which can be used for interferometric filtering, coherence estimation, etc.

4. Experimental Results

In this section, both simulated and real data are used to verify the reliability and effectiveness of the proposed approach.

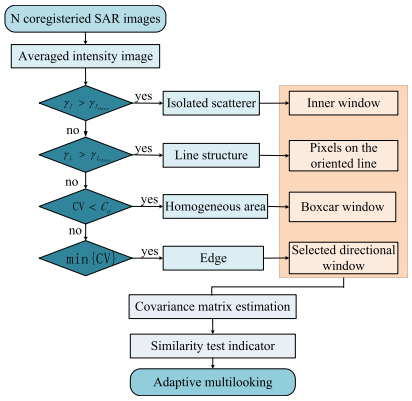

Fig. 1 The flowchart of the proposed AMCV.

(a) (b) (c)

Fig. 2 (a) True amplitude map of the simulated scene. (b) The true average coherence map of the simulated scene. (c) Noisy amplitude map of the first SAR image.

4.1 Simulated Data

The simulated six SAR images of size 430×430 were generated based on TerraSAR-X platform configurations. In this experiment, we consider the regular geometry, comprising of four types of objects with different amplitudes and different scattering stability, as shown in Fig. 2(a). Figure 2(b) presents the true average coherence map of the simulated scene.

For the temporal SAR datasets, the temporal decorrelation is assumed to be exponential decay and the noise components are simulated based on Cholesky decomposition of a predefined coherence matrix. Figure 2(c) presents the noisy amplitude map of the first SAR image. It can be seen that the amplitude map was seriously affected by noise and decorrelation.

Figure 3 presents the average coherence maps estimated by 5×5 boxcar method, 9×9 boxcar method, KS measure, AD measure, PB measure, AMCV, respectively. For the adaptive multilooking, 91 pixels are firstly selected from the search window of size 19×19 pixels based on different distance measures. In the processing of boxcar multilooking, the size of selected window has obvious influences on coherence estimation. Smaller window causes overestimation of coherence in low coherence region, but bigger window reduces spatial resolution of coherence map, as shown in Fig. 3(a) and Fig. 3(b). These problems can be resolved by adaptive multilooking to some degree. The results generated by KS measure, AD measure and PB measure show better spatial

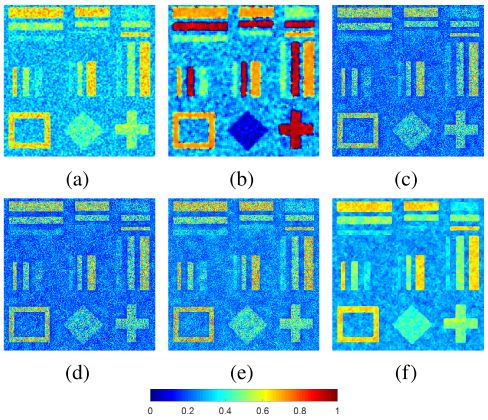

Fig. 3 The average coherence maps of simulated scene generated by (a) the 5×5 boxcar method (b) the 9×9 boxcar method, (c) KS measure, (d) AD measure, (e) PB measure, (f) AMCV.

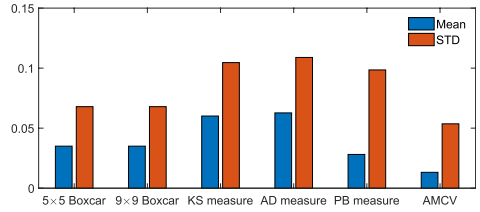

Fig. 4 Quantitative comparison of the average coherence maps shown in Fig. 3.

resolution, but some image details are still blurring. From the visual angle, the mean coherence map generated by the proposed AMCV approach can follow the spatial features of simulated scene and preserve narrow shapes.

To quantitatively analyze the estimated coherence value, the mean value and standard deviation (STD) of the difference between these estimated results and true value are calculated and shown in Fig. 4. It can be seen that the estimated result by AMCV is closest to the reality.

The effects of different stack sizes are also investigated. Figure 5 presents the probability of selection error P_E in the simulated scene when the stack size $N \leq 8$. To ensure the reliability of result, each experiment is repeated ten times. Here, P_E is calculated by $P_E = \frac{N_\Omega}{N_{\bar{\Omega}}}$, where N_Ω and $N_{\bar{\Omega}}$ denote the number of samples and the number of error samples in the selected SHP sets, respectively [8]. It can be seen that the proposed AMCM has a good performance in the case of small data sets and the accuracy of AMCM is relatively stability with reducing stack size.

4.2 Real Data

Five TerraSAR-X stripmap images acquired between March 27, 2009 and September 8, 2009 over the western region of Tianjin, China, were used for experiments with real SAR data. The test region, as shown in Fig. 6(a), covers both towns and countryside intersection. Since the spatial baselines are smaller than 100 m, all of 10 interferograms can be used for SBAS analysis.

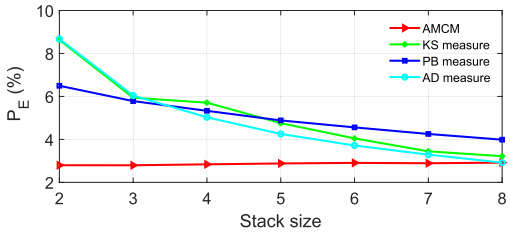

Fig. 5 The probability of selection error P_E with different stack sizes.

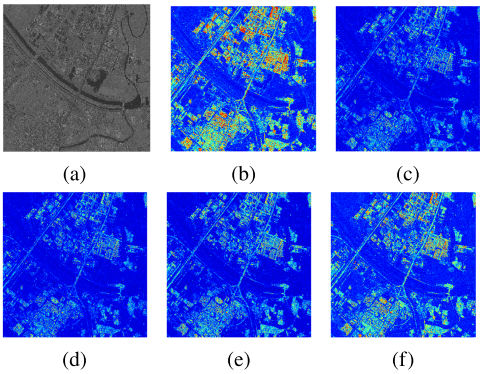

Fig. 6 (a) Average amplitude map of the test region. The average coherence maps of the test region generated by (b) the 9×9 boxcar method, (c) KS measure, (d) AD measure, (e) PB measure, (f) AMCV.

Figure 6(b)–6(e) present the average coherence maps generated by 9×9 boxcar method, KS measure, AD measure, PB measure, AMCV, respectively. The boxcar method caused the loss of spatial resolution and coherence spreading of point-wise scatterers, as shown in Fig. 6(b). The results shown in Fig. 6(c)–6(e) can obtain more details, but the coherence is underestimated because of the unreliable distance measure in the case of stack size $N = 5$. The proposed AMCV approach can effectively mitigate this phenomenon as shown in Fig. 6(f).

5. Conclusions

In this letter, an adaptive multilook approach is presented based on complex covariance matrix. The structure feature in SAR images is firstly detected to adaptively estimate covariance matrix. Compared to amplitude-based methods, the similarity test of covariance matrix is adopted to measure the distance between two pixels. Experimental results both on simulated and real data verify the reliability and effectiveness of the proposed approach.

Acknowledgments

This work was funded by the Open Grant of State Key Laboratory of Complex Electromagnetic Environment Effects on Electronics and Information Systems (CEMEE) under Grant (CEMEE2020K0303B); the National Natural Science Foundation of China (Grant No. 62101167, No. 61901149, No. 61906055); the Natural Science Foundation of Zhejiang

Province under Grant (LQ20D010007).

References

[1] A. Ferretti, C. Prati, and F. Rocca, "Permanent scatterers in SAR interferometry," IEEE Trans. Geosci. Remote Sens., vol.39, no.1, pp.8–20, 2001.

[2] P. Berardino, G. Fornaro, R. Lanari, and E. Sansosti, "A new algorithm for surface deformation monitoring based on small baseline differential SAR interferograms," IEEE Trans. Geosci. Remote Sens., vol.40, no.11, pp.2375–2383, 2002.

[3] A. Hooper, "A multi-temporal InSAR method incorporating both persistent scatterer and small baseline approaches," Geophy. Res. Lett., vol.35, no.16, pp.L16302–L16306, 2008.

[4] A. Hooper, "A distributed scatterers InSAR method based on adaptive window with statistically homogeneous pixel selection for mining subsidence monitoring," Geocarto International, 2022.

[5] A. Ferretti, A. Fumagalli, F. Novali, C. Prati, F. Rocca, and A. Rucci, "A new algorithm for processing interferometric datastacks: SqueeSAR," IEEE Trans. Geosci. Remote Sens., vol.49, no.9, 3460–3470, 2011.

[6] A. Parizzi and R. Brcic, "Adaptive InSAR stack multilooking exploiting amplitude statistics: A comparison between different techniques and practical results," IEEE Geosci. Remote Sens. Lett., vol.8, no.3, pp.441–445, 2011.

[7] M. Jiang, X. Ding, and Z. Li, "Hybrid approach for unbiased coherence estimation for multitemporal InSAR," IEEE Trans. Geosci. Remote Sens., vol.52, no.5, pp.2459–2473, 2014.

[8] F. Sica, G. Reale, L. Poggi, L. Verdoliva, L. Ran, and G. Fornaro, "Nonlocal adaptive multilooking in SAR multipass differential interferometry," IEEE J. Sel. Topics Appl. Earth Observ., vol.8, no.4, pp.1727–1742, 2015.

[9] K. Lin and P. Daniele, "Identification of statistically homogeneous pixels based on one-sample test," Remote Sens., vol.9, no.1, 37, 2017.

[10] M. Jiang, X. Ding, F. Hanssen, R. Malhotra, and L. Chang, "Fast statistically homogeneous pixel selection for covariance matrix estimation for multitemporal InSAR," IEEE Geosci. Remote Sens. Lett., vol.53, no.3, 1213–1224, 2015.

[11] C. Deledalle, L. Denis, and F. Tupin, "How to compare noisy patches? Patch similarity beyond gaussian noise," Int. J. Comput. Vis., vol.99, no.1, pp.86–102, 2012.

[12] C. Deledalle, L. Denis, F. Tupin, and A. Reigber, "NL-SAR: Aunified nonlocal framework for resolution-preserving (POL)(IN)SAR denoising," IEEE Trans. Geosci. Remote Sens., vol.53, no.4, pp.2021–2038, 2015.

[13] J. Goodman, "Statistical properties of laser speckle patterns," Laser Speckle and Related Phenomena, 1963.

[14] M. Schmitt, L. Schönberger, and U. Stilla, "Adaptive covariance matrix estimation for multi-baseline InSAR data stacks," IEEE Trans. Geosci. Remote Sens., vol.52, no.11, pp.6807–6817, 2014.

[15] D. Perissin and A. Ferretti, "Urban-target recognition by means of repeated spaceborne SAR images," IEEE Trans. Geosci. Remote Sens., vol.45, no.12, pp.4043–4058, 2007.

[16] M. Walessa and M. Datcu, "Model-based descpeckling and information extraction from SAR images," IEEE Trans. Geosci. Remote Sens., vol.38, no.5, pp.2258–2269, 2000.

[17] A. Lopes, R. Touzi, and H. Laur, "Structure detection and statistical adaptive speckle filtering in SAR images," J. Remote Sens., vol.14, no.9, pp.1735–1758, 1993.

[18] R. Touzi, "A review of speckle filtering in the context of estimation theory," IEEE Trans. Geosci. Remote Sens., vol.40, no.11, pp.2392–2404, 2002.

[19] W. Hagg and M. Sties, "Efficient speckle filtering of SAR images," Proc. IGARSS, Pasadena, CA, pp.2140–2142, 1994.

[20] J. Lee, K. Papathanassiou, T. Ainsworth, M. Grunes, and A. Reigber, "A new technique for noise filtering of SAR interferometric phase images," IEEE Trans. Geosci. Remote Sens., vol.36, no.5, pp.1456–1465, 1998.

[21] K. Conradsen, A. Nielsen, J. Schou, and H. Skriver, "A test statistic in the complex Wishart distribution and its application to change detection in polarimetric SAR data," IEEE Trans. Geosci. Remote Sens., vol.41, no.1, pp.4–19, 2003.